Research Article

Click chemistry in silico, docking, quantum chemical calculations, and molecular dynamics simulations to identify novel 1,2,4-triazole-based compounds as potential aromatase inhibitors

Alexander M. Andrianov[1] · Grigory I. Nikolaev[2] · Yuri V. Kornoushenko[1] · Sergei A. Usanov[1]

Abstract
Computational development of novel triazole-based aromatase inhibitors (AIs) was carried out followed by investigation of the possible interaction modes of these compounds with the enzyme and prediction of the binding affinity by tools of molecular modeling. In doing so, in silico design of potential AIs candidates fully satisfying the Lipinski's "rule of five" was performed using the concept of click chemistry. Complexes of these drug-like molecules with the enzyme were then simulated by molecular docking and optimized by semiempirical quantum chemical method PM7. To identify the most promising compounds, stability of the PM7-based ligand/aromatase structures was estimated in terms of the values of binding free energies and dissociation constants. At the final stage, structures of the top ranking compounds bound to aromatase were analyzed by molecular dynamic simulations and binding free energy calculations. As a result, eight hits that specifically interact with the aromatase catalytic site and exhibit the high-affinity ligand binding were selected for the final analysis. Six of eight compounds are shown to coordinate the aromatase heme group by the nitrogen–heme–iron interaction typical for triazole-based molecules. At the same time, two compounds form a coordination bond with the heme iron of the enzyme via the lone-pair electrons of their oxygen atoms, which is uncharacteristic for molecules with triazole moieties. All the identified compounds are also involved in multiple van der Waals contacts with the critically important residues of the enzyme hydrophobic pocket, such as Arg-115, Ile-133, Phe-134, Trp-224, Thr-310, Val-370, Met-374, Leu-477, and Ser-478. In addition, most of these compounds form hydrogen bond with Met-374 mimicking the interaction of aromatase with the natural substrate androstenedione, and individual ligands participate in specific π- or T-stacking interactions with the pyrrole rings of the enzyme heme group as well as in hydrogen bonding with Thr-310, Leu-372, Leu-477, and Ser-478. The selected AIs candidates show strong attachment to the enzyme active site, in line with the low values of dissociation constant and binding free energy. Taken together, the data obtained suggest that the identified compounds may present good scaffolds for the development of novel potent drugs against breast cancer.

Keywords Aromatase · Computer-aided drug design · Click chemistry in silico · Molecular docking · Quantum chemistry · Molecular dynamics simulations · Binding free energy calculations · Aromatase inhibitors · Breast cancer

1 Introduction

In women organism during the fertile phase, estrogen synthesis occurs mainly in the ovaries. However, the intensity of estrogen synthesis in the ovaries decreases in postmenopause associated with about a third of cases of breast cancer [1–3]. At this phase, estrogens synthesized in the peripheral tissues using the cytochrome P450 complex, called aromatase. This complex consists of the heme-containing cytochrome P450 (CYP19A1) protein

✉ Alexander M. Andrianov, alexande.andriano@yandex.ru | [1]Institute of Bioorganic Chemistry, National Academy of Sciences of Belarus, Kuprevich Street 5/2, 220141 Minsk, Republic of Belarus. [2]United Institute of Informatics Problems, National Academy of Sciences of Belarus, Surganov Street 6, 220012 Minsk, Republic of Belarus.

SN Applied Sciences (2019) 1:1026 | https://doi.org/10.1007/s42452-019-1051-x

Received: 21 February 2019 / Accepted: 6 August 2019 / Published online: 13 August 2019

and flavoprotein NADPH-cytochrome P450 reductase [1–3]. Aromatase that is encoded by a single large gene, CYP19A1, catalyzes conversion of androgens to estrogens and exhibits biological activity in both peripheral target tissues and in the mammary tumor tissues, providing a high level of estrogen concentration [1–3]. In estrogen-dependent malignant neoplasms, estrogens act as growth factors for tumor development. Therefore, inhibition of aromatase results in a decrease in the level of estrogen in the organism and prevention of the growth and spread of cancer cells [1–3].

In most cases, breast cancer is hormone-dependent. Endocrine therapy of breast cancer is targeted at eliminating the effect of estrogen on a tumor, and its efficacy depends on the expression of estrogen and progesterone receptors by tumor cells. Selective estrogen receptor modulators block the binding of estrogens to their receptors [1–4]. However, they can act as partial agonists or have an estrogenic effect in other tissues, leading to an increased risk of endometrial cancer, gynecological concerns, and thrombotic events. As an alternative strategy, aromatase inhibitors (AIs) that do not have estrogenic effects and cause fewer side effects are used currently in clinical practice for therapy of breast cancer [1, 2, 5]. Catalytic mechanism of aromatase consists in three consecutive hydroxylations of the androgen C-19 methyl group followed by the splitting off formiate and aromatization of the steroid A-ring [2]. Aromatase inhibitors block the aromatization reaction that is a key step in the biosynthesis of estrogens, resulting in suppression of the estrogen synthesis, reduction their level in women body and prevention of the breast cancer development [3–5].

There are three generations of AIs among the drugs for treating hormone-dependent breast cancer [5]. The disadvantage of the drugs of the first two generations (aminoglutethimide, fadrozole, formestane) is the lack of selectivity of action: besides aromatase, these drugs inhibit a number of other enzymes. The third-generation AIs vorozole, letrozole, anastrozole, and exemestane approved for clinical use by the USA Food and Drug Administration (http://www.fda.gov) show greater specificity and efficacy [5]. These inhibitors include drugs of two categories, namely (i) irreversible steroidal inhibitor exemestane that is an androstenedione derivative and (ii) reversible nonsteroidal inhibitors vorozole, anastrozole and letrozole [2, 5]. Steroidal AIs and, in particular, exemestane are transformed by aromatase into compounds that irreversibly bind to the enzyme active site, completely disrupting its activity as a biocatalyst [2, 5]. After the termination of the action of these inhibitors, aromatase needs considerable time to be synthesized in the tissues again. Reversible nonsteroidal AIs vorozole, letrozole and anastrozole are triazole compounds that bind to the catalytic site of the enzyme by coordinating the iron atom of the CYP19A1 heme group through a heterocyclic nitrogen lone pair [3–5]. These third-generation AIs can inhibit aromatase in vivo by > 99% [6], substantially reducing the concentration of estrogens (often down to non-detectable level) [6, 7] and decrease tumor proliferation [8, 9] and growth [10, 11]. The third generation AIs are now the front-line drugs for treating the early and advanced stages of breast cancer in postmenopausal women.

Despite significant progress in the treatment of hormone-dependent breast cancer, this problem has not been completely resolved. Unfortunately, the third-generation AIs cause a number of serious side effects, such as inhibition of muscle growth, arthralgia, decreased bone strength, impaired blood lipid profile, drop *in libido*, as well as deterioration of the general condition [5–11]. In addition, resistance acquired after long-term therapy with these drugs also occurs [12]. In this context, development of novel, more effective and less toxic AIs is of great value.

Modern drug discovery presents the multifaceted process including the identification of small-molecule compounds with strong activity, high selectivity and low toxicity followed by their synthesis, characterization, screening, and assays for therapeutic efficacy [13, 14]. In addition, drug discovery process involves assessment of drug-like properties to identify those compounds that have acceptable ADME parameters (absorption, distribution, metabolism and excretion) and sufficiently acceptable toxicity properties [15, 16]. Drug-like properties are of critical importance for successful design of promising drug candidates [15]. For this reason, one of a key role in drug development belongs to the stage of optimizing the properties of lead compounds that offers significant opportunities to increase their biological activity and pharmacokinetic profile [15].

Until 2009, due to the absence of a crystal structure for human aromatase, new CYP19A1 inhibitors developed using indirect methods of computer-aided drug design based on the identification of common structural elements responsible for the biological activity of known enzyme ligands [17–19]. Determination of the high-resolution X-ray aromatase structure [2, 20] laid the foundation not only for understanding the function and molecular mechanism of the enzyme action, but also for developing new effective CYP19A1 inhibitors by direct methods of computer-aided drug design (e.g., [21–32]).

In the last decade, the methods of molecular modeling have played an ever-increasing role in the design of novel drug compounds [33–37]. The use of computational modeling techniques significantly decreases the time for developing new drug candidates and substantially reduces the average cost of bringing a new drug to market [38]. Computer-aided design of new bioactive compounds can

be performed by virtual screening of molecular databases allowing one to find molecules with the required structural and pharmacophoric features [39–41]. However, the values of their bioactivity usually turn out to be low [40, 41]. Nevertheless, these molecules may serve as good scaffolds for their further optimization aimed at the development of lead compounds with desirable efficiency and pharmacological profile. Furthermore, they also may be used as modular units for the design of novel drug compounds based on the methodology of click chemistry [42–45]. Click-chemistry reactions are modular, stereospecific, wide in scope, result in high yields, and generate only safe by-products [42–45]. These reactions may therefore greatly simplify mass parallel synthesis of drugs candidates and accelerate the development of novel, potent and safe therapeutics. The concept of click chemistry recently has been implemented in a computer program AutoClickChem [46] that can perform click-chemistry reactions in silico and produce large combinatorial libraries of compounds for use in virtual screening. Since the click-chemistry products from such libraries can be easily synthesized for testing in biochemical assays, in silico modeling of these compounds may be very useful in rational drug design and drug optimization [46].

An essential role in structure-based drug discovery belongs to molecular docking that is widely used to predict the ligand conformation and its position and orientation within the binding site of target proteins, assess the binding affinity and investigate the interaction profile of drug candidates [47]. The latest developments of semiempirical quantum mechanical and density functional theory methods as well as applications of explicit quantum mechanical calculations to structure-based drug design in the context of identification and optimization of drug candidates show the growing importance of quantum chemistry in the study of protein–ligand interaction [48–50]. Molecular dynamics (MD) is also a powerful approach for structure-based drug discovery [51]. Unlike molecular docking, MD simulates moving each atom separately in the field of the rest atoms and represents the flexibility of both the ligand and protein more effectively than other algorithms. Examples of successful applications clearly demonstrate the power of computational approaches to identify compounds with desired properties from large databases and design novel small-molecule drug candidates [51].

In this study, computational development of novel triazole-based aromatase inhibitors was carried out followed by evaluation of their antitumor activity by tools of molecular modeling. In doing so, the following studies were performed: (i) in silico design of potential aromatase inhibitor candidates by the AutoClickChem techniques [46], (ii) identification of compounds satisfying the Lipinski's "rule of five" [52] that allows one to recognize molecules with drug-like properties, (iii) molecular docking of these drug-like compounds with the enzyme active site, (iv) refinement of the ligand-binding poses by the PM7 semiempirical quantum chemical method [53], (v) prediction of the interaction modes dominating the binding; (vi) calculation of the values of binding free energy and dissociation constant (K_d) for the PM7-based ligand/CYP19A1 complexes, (vii) prediction of the binding affinity between the identified compounds and aromatase by molecular dynamic simulations and binding free energy calculations, and (viii) selection of molecules most promising for synthesis and biochemical trials.

As a result, eight top ranked compounds that coordinate the iron atom of the aromatase heme group and specifically interact with the catalytic site of the enzyme were identified. Based on the data obtained, these compounds were suggested to present good scaffolds for the development of novel potent drugs against hormone-dependent breast cancer.

2 Methods and computational details

2.1 In silico design of novel CYP19A1 inhibitor scaffolds

The algorithm scheme used in the study is shown in Fig. 1. In the first step, a Drug-Like subset of the ZINC database (http://zinc.docking.org/) [54] was screened by the DataWarrior program (http://www.openmolecules.org/help/basics.html) [55] to generate two virtual compound libraries. Library 1 comprised small molecules (molecular weight < 250 Da) containing 1,2,4-triazole, a popular drug-like azole moiety with a nitrogen atom able to coordinate the Fe^{3+} of the aromatase porphyrin ring [3–5]. In library 2, all low-molecular compounds (molecular mass < 250 Da) with functional groups associated with the current implementation of AutoClickChem [46] were collected. As a result of screening of the ZINC database, a total of 1519 and 2170 compounds were included in libraries 1 and 2, respectively. These small modular units were then used as reactants to mimic click-chemistry reactions by AutoClickChem, resulting in a combinatorial library of 4576 hybrid molecules in which 784 compounds fully satisfied the Lipinski's "rule of five" [52]. These 784 drug-like compounds were further screened by molecular docking and quantum chemical calculations to evaluate the affinity of their binding to the target enzyme.

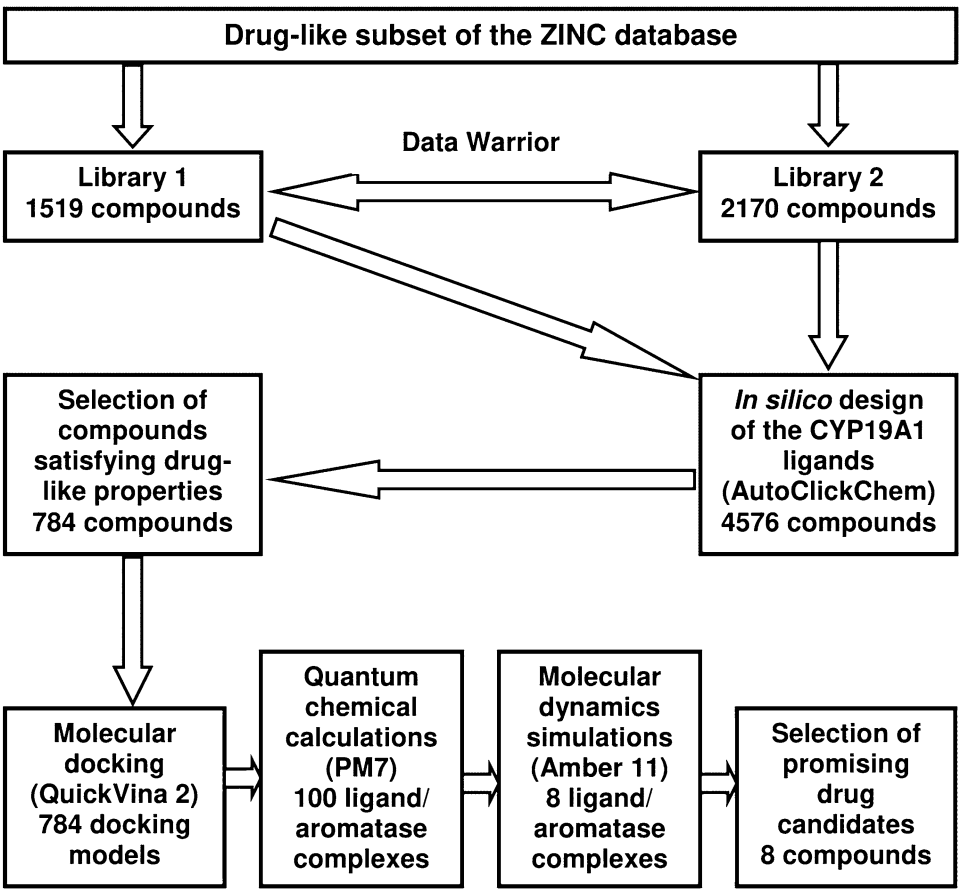

Fig. 1 The algorithm scheme used for identification of potential aromatase inhibitors

2.2 Molecular docking

The X-ray aromatase structure [2, 16] from the PDB file, 3EQM (http://www.rcsb.org/pdb/) [56], was used for rigid receptor and flexible ligand docking with the designed CYP19A1 inhibitor scaffolds by the QuickVina 2 program [57]. At the same time, aromatase inhibitor letrozole was involved in the calculations as a positive control. The 3D letrozole structure from the DrugBank database, DB01006 [58, 59], was used (Fig. 2). The aromatase and ligand structures were prepared by adding hydrogen atoms with the OpenBabel software [60] followed by their optimization in the UFF force field [61]. The designed AIs candidates were docked into the X-ray structure of aromatase [2, 16] using QuickVina 2 [57]. The grid box included the catalytic site of the enzyme and was the region of its crystal structure [2, 16] with the following boundary X, Y, Z values: $X \in (75\ \text{Å}, 95\ \text{Å})$, $Y \in (42\ \text{Å}, 62\ \text{Å})$, $Z \in (34\ \text{Å}, 54\ \text{Å})$; i.e. the box volume was $20\ \text{Å} \times 20\ \text{Å} \times 20\ \text{Å} = 8000\ \text{Å}^3$. The value of "exhaustiveness" parameter defining number of individual sampling "runs" was set to 50 [57]. In all cases, the complexes with the best scores were examined to identify molecules that target the CYP19A1 hydrophobic pocket. Based on the QuickVina 2 scoring function [57], 100 top ranking complexes were selected to be exposed to quantum chemical calculations (Fig. 1). The docked letrozole/CYP19A1 structure was also used in the calculations.

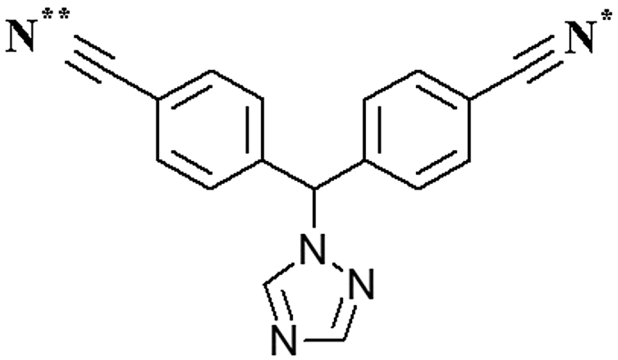

Fig. 2 Chemical structure of letrozole. Atoms making hydrogen bonds with aromatase are marked by asterisks (see the text)

2.3 Quantum chemical calculations

The quantum chemical optimization of the 100 top-ranked docking models was performed by the PM7 semiempirical quantum chemical method [53] in the MOPAC2016

package [62]. Before the calculations, hydrogen atoms were added to the complexes of interest followed by their energy refinement in the UFF force field [61]. In doing so, the Open Babel program [60] was employed. The calculations were carried out by the COSMO solvation model (COnductor-like Screening MOdel) [63–65] using an implicit solvent with water's dielectric constant of 78.4 [62]. The Localized Molecular Orbitals method [66, 67] available in MOPAC in the form of the linear scaling SCF MOZYME algorithm [53, 62] was used to speed up the calculations. The value of RMS gradient was set to 10 kcal/mol/Å [62].

2.4 Analysis of intermolecular interaction profile

Hydrogen bonds, salt bridges, and π–π interactions between the selected compounds and CYP19A1 were analyzed by the BINANA program [68]. Hydrogen bonds were identified with a hydrogen_bond_angle cutoff of 40.0° and a hydrogen_bond_dist_cutoff of 4.0 Å. Salt bridges were detected when the two coordinates corresponding to charges that are opposite were within 5.5 Å of each other [68]. If the centers of two aromatic rings were within 7.5 Å of each other, and the angle between the two vectors normal to the planes of each ring was within 30° of being parallel, π–π stacking interactions were postulated [68]. To identify possible T-stacking interactions, the following criteria were applied: the centers of two aromatic rings are within 5.0 Å of each other, and the angle between the two vectors normal to the planes of each ring is within 30° of being perpendicular [68]. Van der Waals contacts were determined with the use of the program LigPlot [69]. The poses of the molecules in the PM7-based ligand/aromatase structures were visualized by the software package Chimera [70]. The scoring functions of QuickVina 2 [57] and NNScore 2.0 [71] were used to calculate the values of the binding-ligand free energy and K_d, respectively. From the data obtained, 8 complexes with the best QuickVina 2 scores were selected for molecular dynamics simulations and binding free energy calculations (Fig. 1).

2.5 Molecular dynamics simulations

The MD simulations of the ligand/aromatase complexes were carried out using Amber 11 with the implementation of the Amber ff10 force field [72]. The partial atomic charges for ligands were calculated by the Antechamber module of the AmberTools program package [72]. To prepare the force field parameters for ligands, the general Amber force field (GAFF) [73] was applied. The heme prosthetic group was parameterized using the heme (all-atom) parameter set taken from the AMBER parameter database [74]. The tleap module of AmberTools was employed to add hydrogen atoms to aromatase [72]. The MD simulations were performed in truncated octahedron box with periodic boundary conditions using TIP3P water [75] as an explicit solvent. Before the MD simulations, an energy minimization of the system was made with 500 steps of the steepest descent algorithm and 1000 steps of the conjugate-gradient method. An additional harmonic potential with the force constant of 1.0 kcal/mol was imposed on the system atoms and the complex assembly was subject to the equilibration phase. At first, the system was gradually heated from 0 to 310 K for 1 ns in NVT ensemble using a Langevin thermostat with a collision frequency of 2.0 ps^{-1}, and then the pressure equilibration was carried out for 1 ns at 1.0 bar in NPT ensemble using Berendsen barostat with a 2.0 ps characteristic time [72]. At the final stage, the constraints on the complex assembly were removed and the system was equilibrated again at 310 K over 2 ns under constant volume conditions. After equilibration was achieved, the MD simulations were carried out for 60 ns in NPT ensemble at temperature T = 310 K and P = 1 bar. Bonds involving hydrogen atoms were constrained using SHAKE algorithm [76] to achieve the integration time-step of 2 fs. Long-range electrostatic interactions were calculated using Particle Mesh Ewald (PME) algorithm [77]. Coulomb interactions and van der Waals interactions were truncated at 10 Å.

2.6 Binding free energy calculations

The values of binding free energy were calculated with AMBER 11 [73] using the MM/GBSA method [78–80]. The calculations were made for 1000 snapshots extracted from the final 50 ns of the MD trajectories, by keeping the snapshots every 50 ps. The polar solvation energies were computed in continuum solvent using Poisson–Boltzmann continuum-solvation model with ionic strength of 0.1. The non-polar terms were estimated using solvent accessible surface areas [81]. The Nmode module in Amber 11 was applied to calculate the entropy term of the binding free energy [73].

3 Results and discussion

Based on the analysis of the data obtained, eight top-ranked compounds that exhibited the low values of binding free energy (< – 7 kcal/mol) in the PM7-based ligand/aromatase complexes were selected for the final analysis. Depending on the mechanism of binding to the active site of CYP19A1, these compounds were divided into two structural groups designated as groups 1 and 2. Figure 3 sheds light on a scheme of the computer-aided assembly of the hybrid molecules of group 1, and Table 1 presents

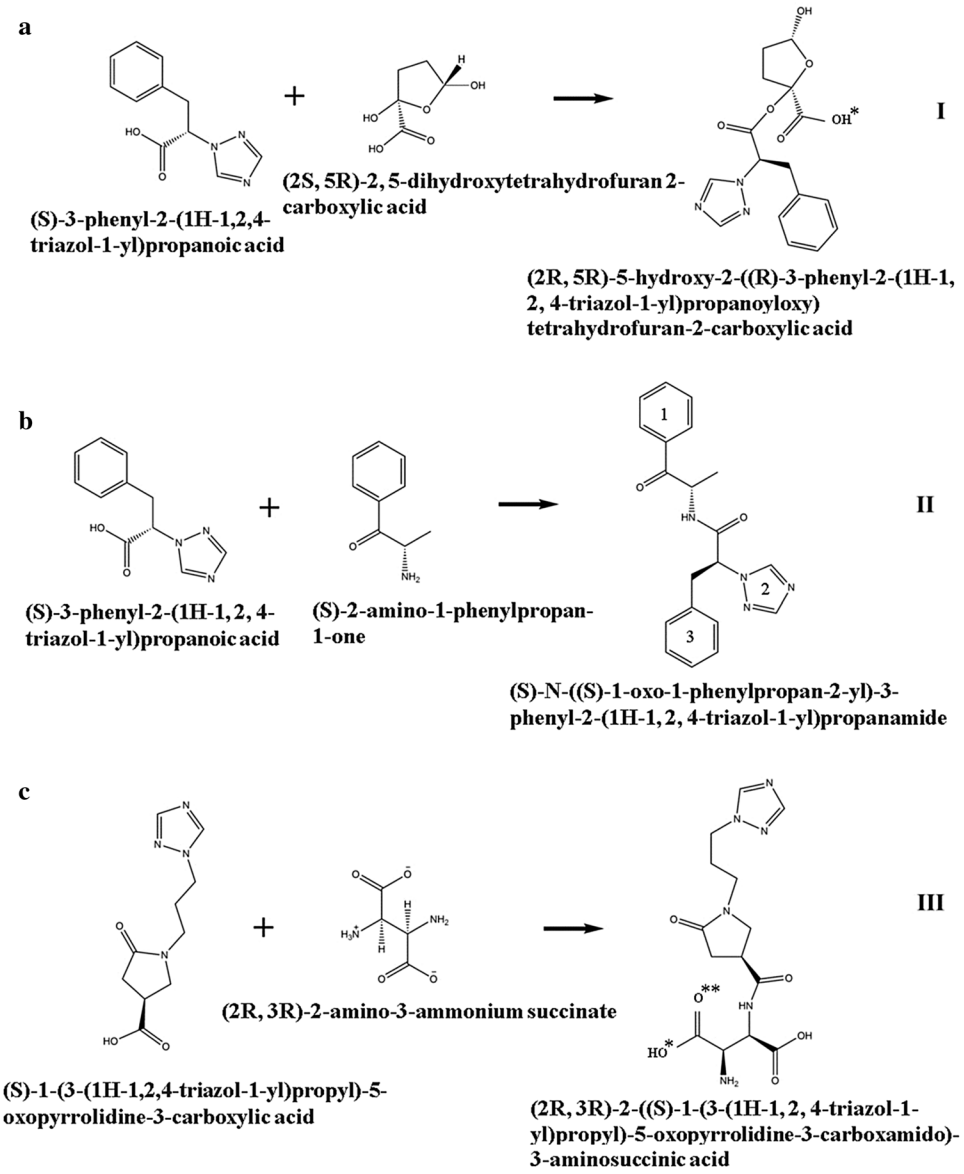

Fig. 3 The scheme of computer-aided assembly of hybrid molecules I (**a**), II (**b**), III (**c**), IV (**d**), V (**e**), VI (**f**) from group 1. Reagents and reaction products are shown. Systematic names of these compounds are given. The molecule functional groups forming hydrogen bonds with aromatase are indicated by superscripts * and **; π-conjugated systems of the ligands involved in π–π interactions with the pyrrole rings of the CYP19A1 heme group are marked by numerals 1, 2, 3. These designations are used in Table 2 in which information on the intermolecular interaction profile for the compounds of group 1 is given (see also note to this Table). Compounds I–VI were designed by computer-based simulation of the following reactions: esterification (**a**), amidification (**b**, **c**, **d**), transesterification (**e**), and thioesterification (**f**)

their ADME characteristics providing such important properties for a drug as absorption, distribution, metabolism and excretion. As follows from the data of Table 1, all the molecules of interest fully satisfy the criteria imposed on potential drug by Lipinski's "rule of five" [52].

Anaysis of the structural complexes of the identified compounds with aromatase (Fig. 4) shows that one of the nitrogen atoms of the triazole ring forms a coordinate bond with the heme iron, as evidenced by the interatomic distances Fe–N (Table 2). The predicted Fe–N distances given in Table 2 are in good agreement with the crystallographic data on the lengths of coordination bonds between iron and nitrogen in six-coordinated iron binding sites [82]. From these data, typical Fe–N distances range between 1.9 and 2.1 Å for sites with a low-spin iron, while they change from 2.1 to 2.3 Å for sites with a high-spin iron that occur upon substrate binding [82], indicating a high probability of realizing the nitrogen–heme–iron interaction between the analyzed compounds and the active site of aromatase. According to the predicted binding modes, compounds I, III–VI form hydrogen bond with residue Met-374 mimicking the interaction of aromatase with the natural substrate androstenedione. According to the X-ray data [2, 20], one of the oxygen atoms of the androstenedione D-ring is involved in the H-bonding with Met-374 NH. In addition, ligand IV forms hydrogen bonds with the aromatase residues Thr-310 and Leu-372 as well as with the nitrogen atom of the heme. Besides, ligand III forms a salt bridge with Arg-115, and compound V participates in the H-bonding with Leu-477 and Thr-310 (Table 2). In this context, it should be noted that Thr-310 is a highly conserved residue

Fig. 3 (continued)

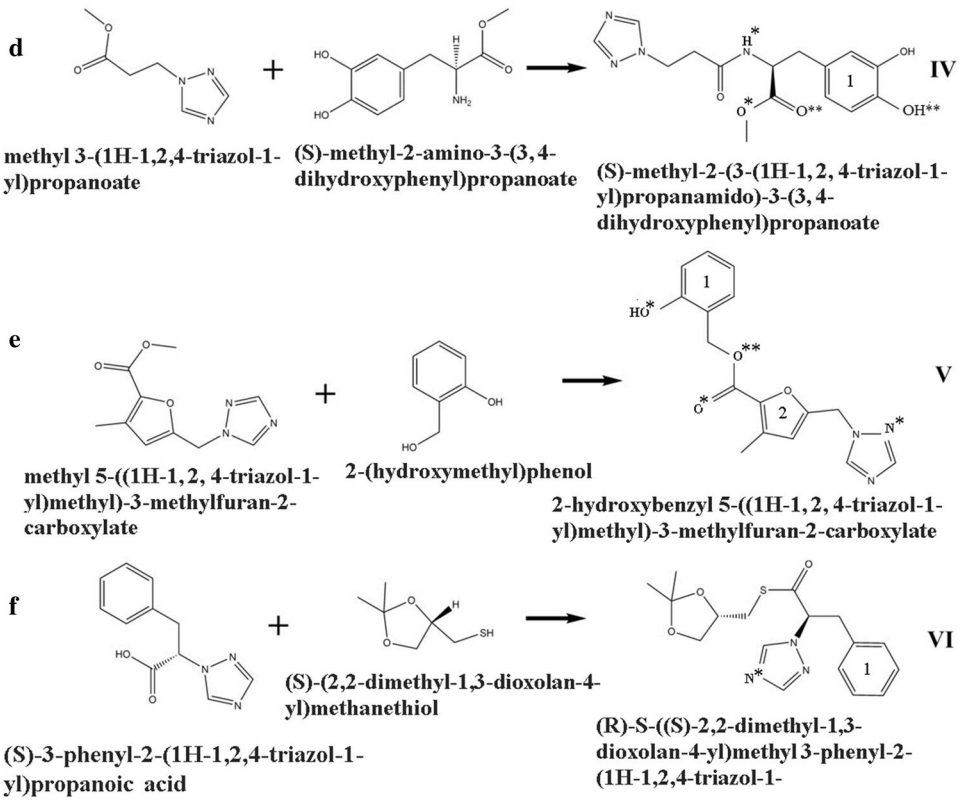

Table 1 Physicochemical parameters of the compounds of group 1 associated with the Lipinski's "rule of five"

Compound	Chemical formula	Molecular mass (Da)	LogP[a]	Number of H-bond donors	Number of H-bond acceptors	Volume (Å^3)
I	$C_{16}H_{17}N_3O_6$	347.3	0.03	2	9	297.9
II	$C_{20}H_{20}N_4O_2$	348.4	2.04	1	6	318.9
III	$C_{14}H_{18}N_6O_6$	367.3	−4.88	3	12	286.9
IV	$C_{15}H_{18}N_4O_5$	334.3	−1.03	3	9	292.1
V	$C_{16}H_{15}N_3O_4$	313.3	1.38	1	7	269.6
VI	$C_{17}H_{21}N_3O_3S$	347.4	2.07	0	6	316.0

The data given are obtained by the DruLiTo software (http://www.niper.gov.in/pi_dev_tools/DruLiToWeb/DruLiTo_index.html)

[a]The compound lipophilicity

in P450s and, together with Ala-306, plays an important role in the hydroxylation reactions [2, 20].

Along with hydrogen bonds, all the identified compounds are involved in multiple van der Waals interactions with the hydrophobic pocket lined by conservative residues Arg-115, Ile-133, Phe-134, Trp-224, Thr-310, Val-370, Met-374, Leu-477, and Ser-478 (Table 2, Fig. 5). In addition, individual compounds of group 1 participate in van der Waals interactions with the aromatase residues Leu-372 (compounds I, II, IV, V, VI), Val-373 (compounds I–V), Phe-221 (compounds I, II, III, VI), Ala-306 (compounds II–V) and Val-369 (compound I) (Table 2, Fig. 5). At the same time, the total number of van der Waals contacts of these ligands with the substrate-binding site of CYP19A1 varies from 32 (compound III) to 62 (compound II). It is known that the above residues are extremely important for the catalytic activity of CYP19A1 [5]. In particular, extensive site-directed mutagenesis experiments indicate that mutations of Ser-478 to alanine or threonine affect letrozole and anastrozole binding [83]. The data on the crystal structure of aromatase show [2, 20] that the Phe-221, Trp-224 and Met-374 residues are of great importance for binding of the androgen substrate as well as AIs, which is also confirmed by site-directed mutagenesis [83]. Furthermore, the residue Trp-224 participates in the mechanism-based

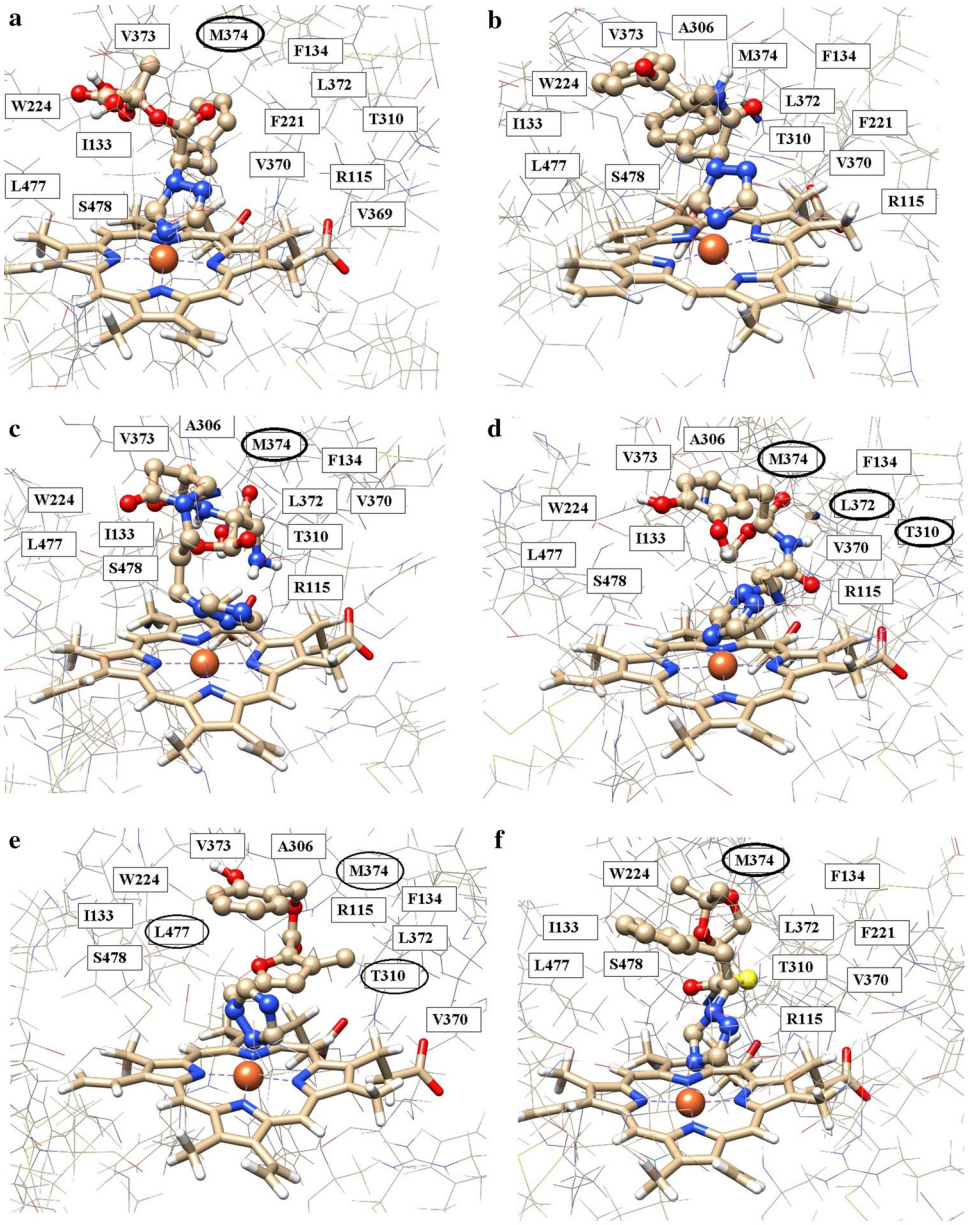

Fig. 4 The PM7-based structures of compounds I (**a**), II (**b**), III (**c**), IV (**d**), V (**e**), and VI (**f**) from group 1 bound to aromatase. The compounds are shown using "ball-stick-ball" model. The residues of CYP19A1 forming van der Waals contacts with ligands are located in rectangles (Table 2). The residues involved in the hydrogen bonding are marked by an ellipse

inhibition of activity by exemestane, as time-dependent inhibition is eliminated with mutation on this residue [84].

The data obtained suggest that the designed molecules (Fig. 3) may interact not only with the amino-acid residues of the aromatase active site, but also with the heme group of this enzyme. Except ligand III, these small molecules form van der Waals contacts with the CYP19A1 heme group, and π-conjugated systems of compounds II, IV, V, and VI (Fig. 3) are involved in specific π–π interactions with its pyrrole rings (Table 2).

Thus, analysis of the intermolecular interaction profile calculated for the ligand/aromatase structures indicates that the identified AIs candidates exhibit close mode of binding to the aromatase active site. This binding is generally provided by the nitrogen–heme–iron interaction, multiple van der Waals contacts, hydrogen bonds (compounds I, III–VI), salt bridges (compound III) and π-stacking between π-conjugated systems of the ligands and pyrrole rings of the heme group (compounds II, IV, V, VI) (Table 2, Fig. 5). Among these binding modes, intermolecular van der Waals interactions are the major contributors to the ligand/aromatase interface including both conservative amino-acid residues of the CYP19A1 active site and the structural elements of the enzyme heme group (Table 2, Fig. 5). The efficiency of intermolecular interactions appearing in the ligand/aromatase structures is supported by the low values of binding free energy and K_d (Table 3).

Table 2 Intermolecular interaction profile calculated for the compounds of group 1 and letrozole bound to aromatase

Compound	Hydrogen bonds[a]	Van der Waals contacts[b]	Salt bridges and π–π interactions[c]	Length of the N–Fe bond[d] (Å)
I	OH*…N[M374]	R115(3), I133(4), F134(3), F221(3), W224(3), T310(4), V369(6), V370(2), L372(3), V373(1), M374(1), L477(3), S478(1), HEME (8)	–	1.99 (4)
II	–	R115(3), I133(1), F134(1), F221(1), W224(2), A306(3), T310(2), V370(8), L372(1), V373(6), M374(1), L477(7), S478(4), HEME (22)	1…HEME 2… HEME 3… HEME (π-stacking)	2.01 (4)
III	O*…NH[M374] O**…NH[M374]	R115(4), I133(2), F134(2), F221(1), W224(2), A306(3), T310(5), V370(1), V373(1), M374(1), L477(7), S478(3)	OCO…R115 (salt bridge)	2.38 (2)
IV	O*…NH[M374] O**…OH[T310] OH**…N[HEME] NH*…O[L372]	R115(3), I133(4), F134(1), W224(2), A306(2), T310(1), V370(2), L372(4), V373(1), M374(1), L477(5), S478(2), HEME (14)	1… HEME (π-stacking)	2.01 (4)
V	O*…NH[M374] O**…NH[M374] OH*…O[L477] N*…OH[T310]	R115(2), I133(4), F134(2), W224(1), A306(1), T310(4), V370(4), L372(2),V373(5), M374(1), L477(4), S478(6), HEME (17)	1… HEME 2… HEME (π-stacking)	1.81 (2)
VI	N*…NH[M374]	R115(6), I133(2), F134(4), F221(3), W224(4), T310(2), V370(5), L372(1), M374(6), L477(5), S478(2), HEME (18)	1… HEME (π-stacking)	2.01 (4)
Letrozole	N*…OH [S478] N**…NH [M374]	R115(2), F134(2), F221(7), W224(6), A306(1), D309(8), T310(6), V369(2), V370(1), M374(2), L477(3), S478(3), H480(1), HEME (6)	–	1.95 (4)

[a]Donors and acceptors of the hydrogen bonds relating to the ligands are shown first, followed by the corresponding functional groups of the aromatase amino-acid residues. The residues of aromatase are in square brackets in one-letter code. Superscripts * and ** for oxygen, nitrogen and hydrogen atoms match their designations in Fig. 3

[b]Amino acids of aromatase forming van der Waals contacts with the ligands. The number of the contacts is shown in round brackets

[c]The ligand functional groups and numbers of their aromatic rings marked as shown in Fig. 3 are given first for salt bridges and π–π interactions, respectively

[d]The length of the coordinate bond between a heterocyclic nitrogen and the iron atom of the heme group of the enzyme. The number of nitrogen atom is indicated in round brackets

In the case of letrozole used in the study as a control, the methods of molecular modeling predict a mechanism of binding to aromatase similar to that of described above for the designed 1,2,4-triazole-based compounds of group 1. With the calculated data (Table 2, Fig. 6), this CYP19A1 inhibitor coordinates the iron atom of the enzyme heme, forms hydrogen bonds with Met-374, Ser-478 and a large number of van der Waals contacts with such functionally important residues as Arg-115, Phe-134, Trp-224, Thr-310, Val-370, Met-374, Leu-477, and Ser-478. It is those amino-acid residues of CYP19A1 that are also involved in the direct interatomic interactions with the analyzed compounds (Table 2, Figs. 5, 6). Importantly, the K_d value of 7.66 nM calculated for the letrozole/aromatase complex (Table 3) is close to that of 3.03 nM measured for this supramolecular structure by differential spectrophotometry [85], indicating good prediction accuracy of the computational algorithm used in the calculations.

Figure 7 shows a scheme of the computer-aided assembly of the compounds of group 2, and Table 4 presents brief information on these molecules. Analysis of the data in Table 4 indicates that these potential ligands of CYP19A1 are also small molecules exhibiting drug-like properties [52]. However, unlike the ligands of group 1, the triazole ring of these compounds does not form a coordinate bond with the iron atom of the enzyme heme (Table 5, Figs. 8, 9). In this case, the coordination occurs by the donor–acceptor interactions of the heme iron atom with the oxygen atoms of the analyzed molecules (Table 5, Fig. 8). For these molecules, van der Waals contacts of their triazole ring with conservative residues of the aromatase hydrophobic pocket are likely to be more energetically preferable than the nitrogen–heme–iron interaction typical for triazole-based compounds [e.g., 84, 86]. Really, inspection of Table 5 and Fig. 8 reveals a wide network of van der Waals contacts between triazole cycle of the molecules of interest and the pivotal residues of the CYP19A1 catalytic site, such as Arg-115, Ile-133, Phe-221, Trp-224, Thr-310, Val- 370, Met-374, Leu-477, Ser-478 (Table 5) [2, 20, 83, 84]. In addition, compound II is involved in specific π–π interactions with the pyrrole rings of the CYP19A1 heme, makes T-stacking with the π-conjugated system

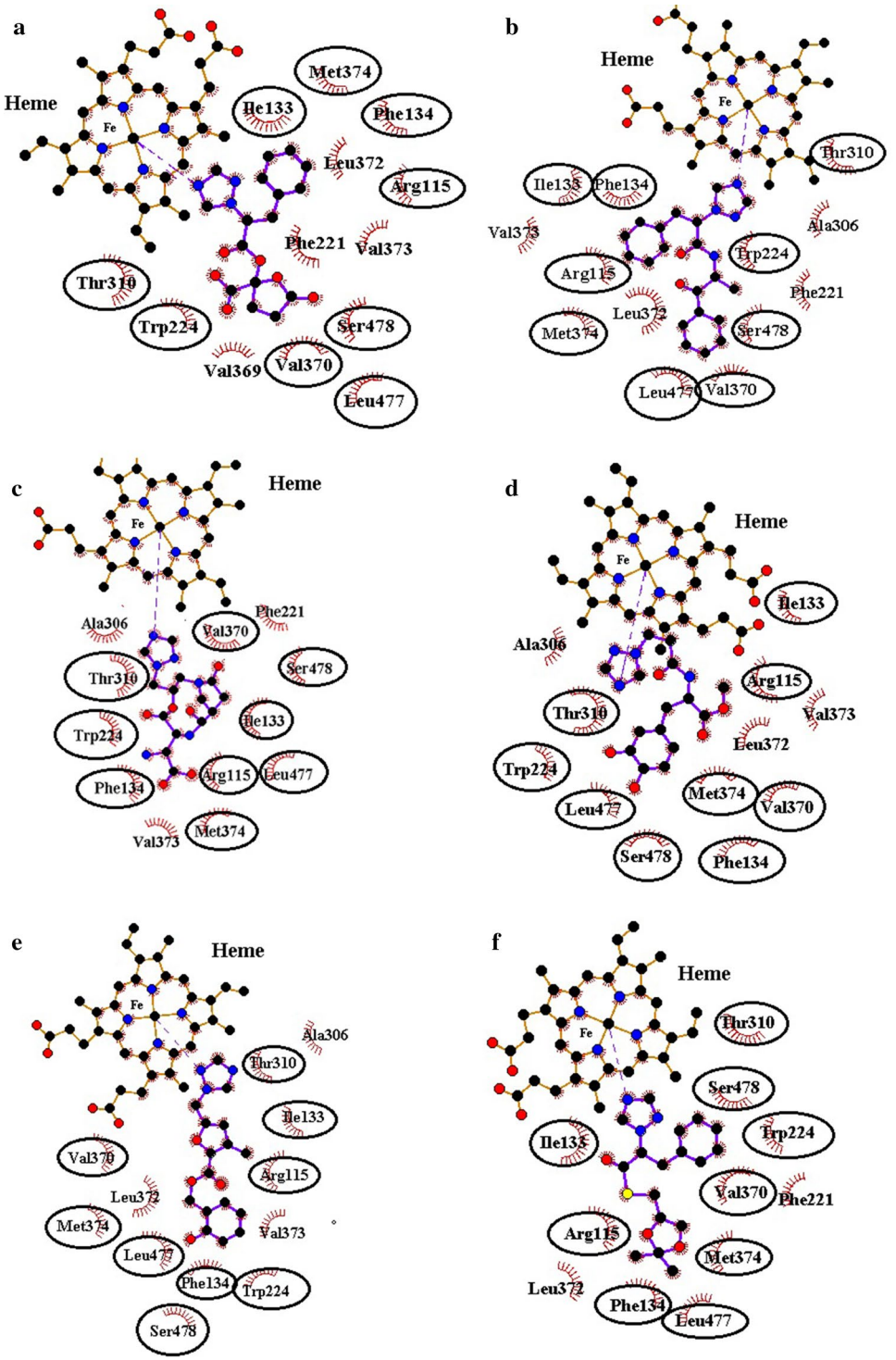

Fig. 5 The aromatase residues making van der Waals contacts with compounds I (**a**), II (**b**), III (**c**), IV (**d**), V (**e**), and VI (**f**) from group 1. Residues involved in van der Waals interactions in all of the cases of interest are marked by an ellipse. The total number of van der Waals contacts is: 45 (**a**), 62 (**b**), 32 (**c**), 42 (**d**), 53 (**e**) and 58 (**f**). The nitrogen–heme–iron interaction is shown by dotted line

Table 3 Values of binding free energy (ΔG) and K_d for the compounds of group 1 and letrozole bound to aromatase

Compound	I	II	III	IV	V	VI	Letrozole
ΔG (kcal/mol)	−7.8	−9.2	−8.8	−8.1	−8.7	−8.0	−8.7
K_d (nM)	12.21	38.35	43.24	51.07	64.39	73.72	7.66

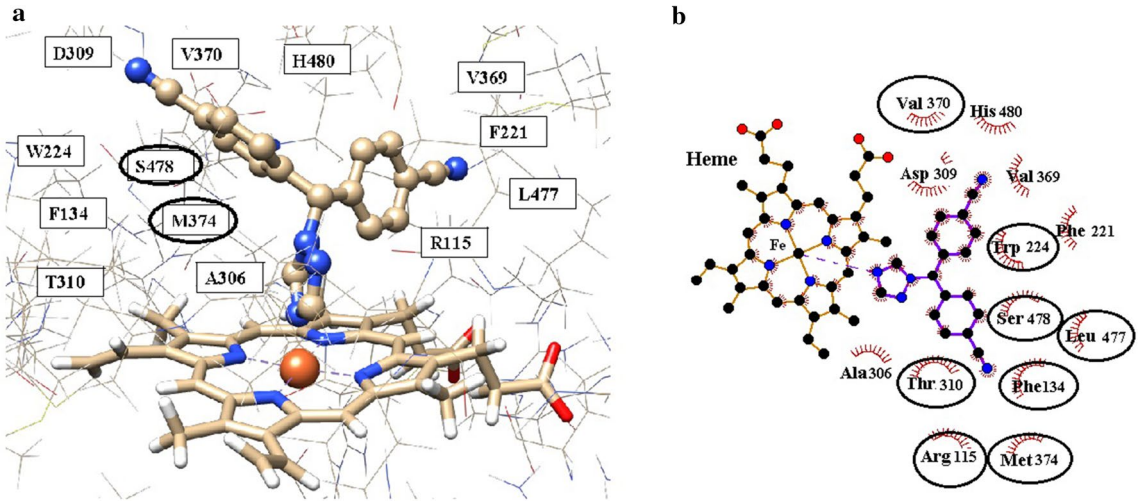

Fig. 6 The PM7-based letrozole/aromatase structure (**a**) and residues of CYP19A1 involved in van der Waals interactions (**b**). **a** Letrozole is shown using "ball-stick-ball" model. The residues of CYP19A1 forming van der Waals contacts with ligands are located in rectangles (Table 2). The residues involved in the hydrogen bonding are marked by an ellipse. **b** The residues of aromatase participating in van der Waals interactions both with letrozole and the ligands of group 1 are marked by an ellipse. The total number of van der Waals contacts is 50. The nitrogen–heme–iron interaction is shown by dotted line

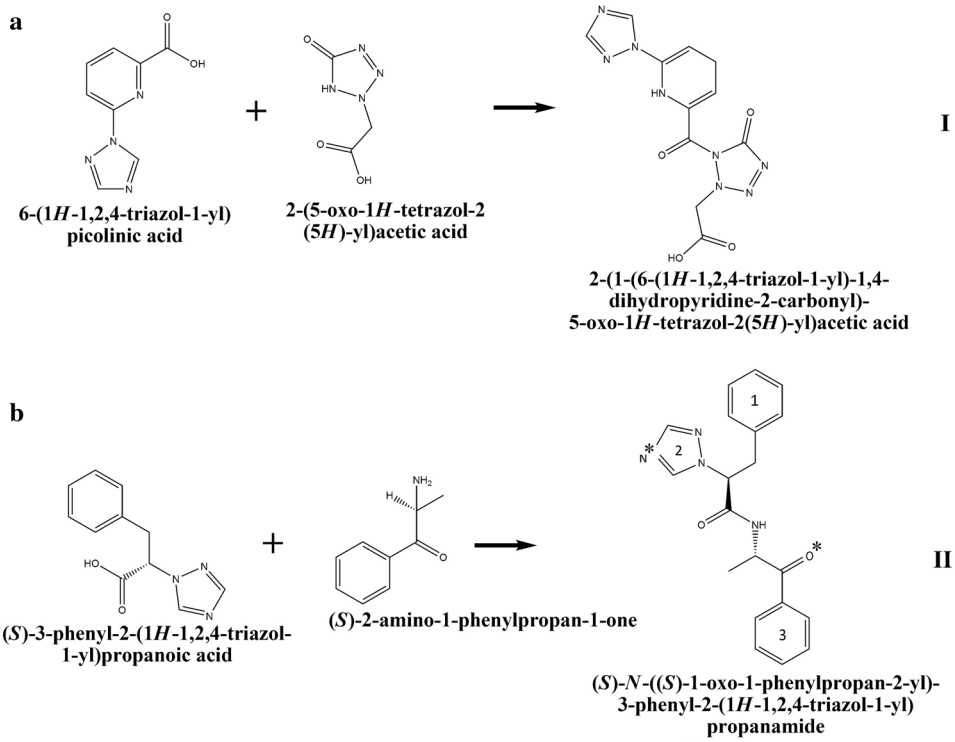

Fig. 7 The scheme of computer-aided assembly of the hybrid molecules I (**a**) and II (**b**) from group 2. Reagents and reaction products are shown. Systematic names of these compounds are given. Oxygen and nitrogen atoms of compound II forming hydrogen bonds with CYP19A1 are indicated by superscript *; π-conjugated systems of ligand II involved in π–π interactions with the pyrrole rings of the CYP19A1 heme group are marked by numerals 1, 2, 3. These designations are used in Table 5 in which the information on the intermolecular interaction profile for the compounds of group 2 is given (see also note to this Table). Compounds were designed by an amidification reaction

Table 4 Physicochemical parameters of the compounds of group 2 associated with the Lipinski's "rule of five"

Compound	Chemical formula	Molecular mass (Da)	LogP[a]	Number of H-bond donors	Number of H-bond acceptors	Volume (Å^3)
I	$C_{11}H_{10}N_8O_4$	318.2	3.80	2	12	251.7
II	$C_{20}H_{20}N_4O_2$	348.4	2.04	1	6	314

[a]The compound lipophilicity

Table 5 Intermolecular interaction profile calculated for the compounds of group 2 bound to aromatase

Compound	Hydrogen bonds	Van der Waals contacts[b]	Salt bridges and π–π interactions[c]	Length of the coordinate bond[d] (Å)
I	–	R115(3), F134(2), I133(2), F221(1), W224(2), A306(1), T310(4), V370(2), M374(4), L477(2), S478(1), HEME(15)	CO_2…HEME (salt bridge)	2.15 (O)
II[a]	N*…NH[M374] O*…OH[T310]	R115(1), F134(1), I133(5), F221(5), W224(8), E302(1), I305(2), A306(8), T310(5), V370(4), L372(1), M374(2), L477(2), S478(2), HEME(1)	1…HEME (π-stacking) 2…F134 3…HEME (T-stacking)	1.87 (O)

[a]Acceptors of the hydrogen bonds relating to the ligands are shown first, followed by the corresponding H-bond donors of the aromatase amino-acid residues. The residues of aromatase are in square brackets in one-letter code. Superscripts of oxygen and nitrogen atoms match their designations in Fig. 7

[b]Amino acids of aromatase forming van der Waals contacts with the ligands. The number of the contacts is shown in round brackets

[c]Numerals of the aromatic rings of ligand II as marked in Fig. 7 are shown first

[d]The length of the coordinate bond between the iron atom of the heme group and the oxygen atoms in compounds I and II. The type of the ligand atom bonded to the heme iron is indicated in round brackets

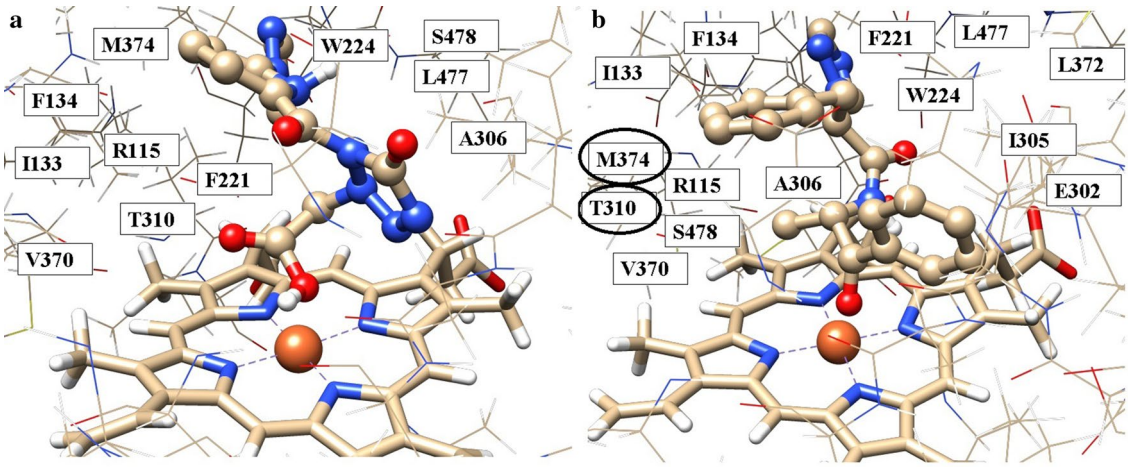

Fig. 8 The PM7-based structures of compounds I (**a**) and II (**b**) from group 2 bound to aromatase. The compounds are shown using "ball-stick-ball" model. The residues of CYP19A1 forming van der Waals contacts with ligands are located in rectangles (Table 5). The residues involved in hydrogen bonding are marked by an ellipse

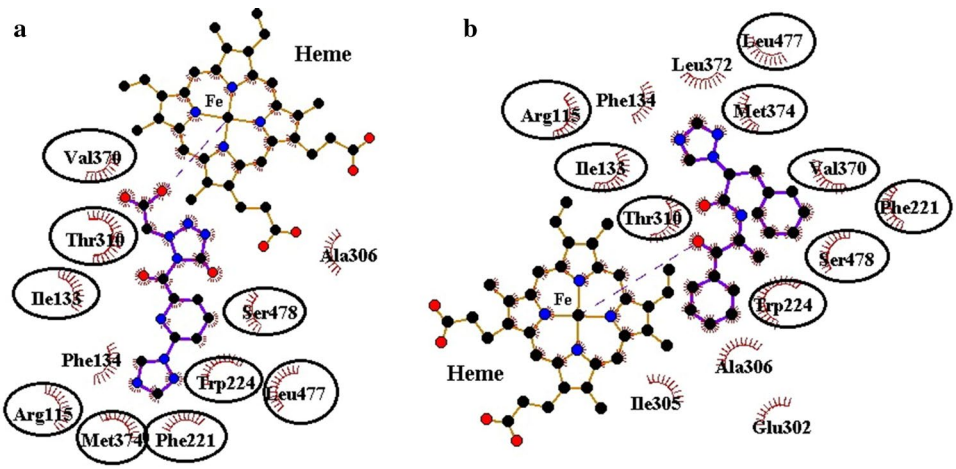

Fig. 9 The aromatase residues making van der Waals contacts with compounds I (**a**) and II (**b**) from group 2. Residues involved in van der Waals interactions in both cases are marked by an ellipse. The total number of van der Waals contacts is 39 (**a**) and 48 (**b**). The donor–acceptor interaction is shown by dotted line

of the Phe-134 side chain and hydrogen bonds with residues Met-374 and Thr-310. Besides, compound I forms a salt bridge with the aromatase heme (Table 5). Finally, analysis of the data of Table 6 indicates that, like the molecules from group 1, the compounds of group 2 exhibit a high binding affinity in the complexes with aromatase, as evidence with the low values of dissociation constant and binding free energy.

Molecular dynamics insights into the ligand/aromatase complexes validate the main findings derived from the analysis of their static structures. These complexes are relatively stable during the MD simulations, which is supported by the averages of binding free energies, their enthalpic components, and corresponding standard deviations (Table 7). Given the accuracy of the MM/GBSA method evaluated in studies [78–80], one can suppose that the averages of binding free energy predicted for the designed compounds in the complexes with aromatase are comparable with the value calculated for the letrozole/aromatase complex by the identical computational protocol (Table 7). Furthermore, these averages are also comparable with the values estimated by QuickVina 2 [59] for the static models of the ligand/aromatase complexes (Tables 3, 6) as well as to that of -12.06 kcal/mol obtained with the formula $\Delta G = R \times T \times \ln(K_d)$ at temperature T = 310 K) [87] using the experimental value of K_d for letrozole bound to aromatase [85].

So, the analysis of the obtained results shows that all identified compounds (Figs. 3, 7) may specifically and effectively block the structural elements of the aromatase active site critical for its catalytic activity, which is confirmed by the low values of binding free energy and K_d (Tables 3, 6, 7). However, when analyzing the data of Tables 3, 6 and 7, it is necessary to keep in mind that all computational approaches for estimating the binding affinity involve various approximations. They vary from simplified forms of the first-principles equations that are easier or faster to solve, to approximations limiting the size of the system (for example, periodic boundary conditions), to fundamental approximations to the underlying equations that are required to achieve any solution to them at all. However, the accuracy of the recent quantum chemical method PM7 [53], the only semiempirical method taking into account corrections for intermolecular dispersion interactions and hydrogen bonds [53, 88], gives reason to assume that the values of binding free energy and K_d (Tables 3, 6) enable one to make a correct prediction of the binding affinity between the designed compounds and aromatase. This assumption is also supported by the data on the accuracy of binding affinity prediction provided by QuickVina 2 [57], NNScore 2.0 [71] and MM/GBSA [78–80] as well as by the results of a recent study [89], whereby the use of quantum chemical semiempirical method PM7 for optimization of the ligand/protein complexes simulated based on classical force field significantly improves the ligands positioning accuracy.

Table 6 Values of binding free energy (ΔG) and K_d for the compounds of group 2 bound to aromatase

Compound	I	II
ΔG (kcal/mol)	−8.7	−8.6
K_d (nM)	22.38	30.30

Table 7 Averages of binding free energy (⟨ΔG⟩) for the complexes of the AIs candidates and letrozole with aromatase and their standard deviations (ΔG_{STD})

Compound	⟨ΔH⟩ (kcal/mol)	$(\Delta H)_{STD}$ (kcal/mol)	⟨TΔS⟩ (kcal/mol)	$(T\Delta S)_{STD}$ (kcal/mol)	⟨ΔG⟩ (kcal/mol)	ΔG_{STD} (kcal/mol)
Compounds of group 1						
I	−32.2	4.0	−22.6	2.9	−9.6	3.4
II	−28.3	5.7	−16.4	4.0	−11.9	4.8
III	−35.2	5.6	−23.9	6.2	−11.3	5.9
IV	−26.8	4.5	−17.9	3.4	−8.9	3.9
V	−25.7	5.5	−16.1	3.6	−9.6	4.4
VI	−28.4	4.6	−19.7	3.6	−8.7	4.0
Compounds of group 2						
I	−27.9	3.5	−18.5	3.7	−9.4	3.6
II	−24.8	3.6	−16.5	5.5	−8.3	4.5
Letrozole						
	−37.3	4.3	−27.0	9.6	−10.3	6.4

⟨ΔH⟩ and ⟨TΔS⟩are the mean values of enthalpic and entropic components of free energy, respectively; $(\Delta H)_{STD}$ and $(T\Delta S)_{STD}$ are standard deviations corresponding to these values

4 Conclusions

The data of molecular modeling indicate that each of the identified compounds of group 1 shows peculiar interactions with the enzyme binding pocket, the interaction being realized between the triazole ring and the heme iron, van der Waals interactions with the hydrophobic pocket lined by Arg-115, Ile-133, Phe-134, Trp-224, Thr-310, Val-370, Met-374, Leu-477, Ser-478, and, except compound II, the hydrogen bond with Met-374, which is also involved in hydrogen bonding with the natural substrate androstenedione. In addition, some identified compounds form van der Waals contacts with the heme of CYP19A1, and π-conjugated systems of individual molecules participate in specific π–π interactions with the pyrrole rings of the heme group. Finally, the selected AIs candidates expose strong attachment to the enzyme active site, in line with the low values of binding free energy and K_d. In summary, the conclusions that can be made by the new identified AIs are that, in addition to the interaction between the triazole rings and the heme iron, hydrophobic contacts play a pivotal role in the ligand binding, and hydrogen bond involving Met-374 is also essential for the ligand recognition.

Unlike the molecules of group 1, the ligands of group 2 demonstrate a mechanism of binding to aromatase uncharacteristic for triazole-based compounds generally coordinating the iron atom of the heme via a heterocyclic nitrogen lone pair. According to the calculated data, the ligands of interest coordinate the iron atom of the CYP19A1 heme group through the lone pairs of their oxygen atoms. Similarly to the molecules of group 1, all these compounds target the well-conserved hotspots of the aromatase catalytic site using multiple van der Waals interactions with the critically important residues of this hydrophobic pocket. Besides, compound II participates in specific π–π interactions with the pyrrole rings of the CYP19A1 heme group and form hydrogen bonds with residues Met-374 and Thr-310, and compound I forms a salt bridge with the enzyme heme.

Finally, analysis of the ligand/aromatase complexes indicates a high binding affinity between the identified compounds and the enzyme, in agreement with the low values of binding free energy calculated both for their static and dynamic models. Certainly, the above computational findings are a prediction and their final confirmation can be obtained only after testing the designed compounds for antitumor activity. Unfortunately, synthetic methodologies still limit the compounds that computational chemists can design [90]. However, eight compounds identified in this study can be synthesized by quite simple click chemistry reactions using commercially available modular units as reactants (Figs. 3, 7) [46]. This work is now in progress and its further advancement proposes to use these AIs mimetic candidates as the fixed scaffolds for computer-based generation of their modified forms with improved biological activity and drug-like properties (e.g., [91, 92]) followed by synthesis and detailed biochemical assays.

Acknowledgements This study was supported by a grant of the State Program of Scientific Research "Chemical Technologies and Materials" (subprogram 2.2 "Biologically active compounds", Project 2.15).

Compliance with ethical standards

Conflict of interest The authors declare that they have no competing interests.

References

1. Macedo LF, Sabnis G, Brodie A (2009) Aromatase inhibitors and breast cancer. Ann N Y Acad Sci 1155:162–173
2. Ghosh D, Griswold J, Erman M, Pangborn W (2009) Structural basis for androgen specificity and oestrogen synthesis in human aromatase. Nature 457(7226):219–223
3. Hong Y, Chen S (2006) Aromatase inhibitors: structural features and biochemical characterization. Ann N Y Acad Sci 1089:237–251
4. Dutta U, Pant K (2008) Aromatase inhibitors: past, present and future in breast cancer therapy. Med Oncol 25(2):113–124
5. Ghosh D, Lo J, Egbuta C (2016) Recent progress in the discovery of next generation inhibitors of aromatase from the structure–function perspective. J Med Chem 59:5131–5148
6. Lonning PE (1996) Pharmacology of new aromatase inhibitors. The Breast 5:202–206
7. Geisler J, Haynes B, Anker G, Dowsett M, Lønning PE (2002) Influence of letrozole and anastrozole on total body aromatization and plasma estrogen levels in postmenopausal breast cancer patients evaluated in a randomized, cross-over study. J Clin Oncol 20:751–757
8. Dowsett M (2003) Preoperative models to evaluate endocrine strategies for breast cancer. Clin Cancer Res 9:502S–510S
9. Anderson TJ, Dixon JM, Stuart M, Sahmoud T, Miller WR (2002) Effect of neoadjuvant treatment with anastrozole on tumor histology in postmenopausal women with large operable breast cancer. Br J Cancer 87:334–338
10. Dixon JM (2002) Neoadjuvant therapy: surgical perspectives. In: Miller WR, Ingle JN (eds) Endocrine therapy in breast cancer. Marcel Dekker, New York, pp 197–212
11. Miller WR, Jackson J (2003) The therapeutic potential of aromatase inhibitors. Expert Opin Investig Drugs 12:1–12
12. Johnston SR, Martin LA, Head J, Smith I, Dowsett M (2005) Aromatase inhibitors: combinations with fulvestrant or signal transduction inhibitors as a strategy to overcome endocrine resistance. J Steroid Biochem Mol Biol 95:173–181
13. Guido RV, Oliva G, Andricopulo AD (2011) Modern drug discovery technologies: opportunities and challenges in lead discovery. Comb Chem High Throughput Screen 14:830–839
14. Chen J, Luo X, Qiu H, Mackey V, Sun L, Ouyang X (2018) Drug discovery and drug marketing with the critical roles of modern administration. Am J Transl Res 10:4302–4312

15. Kerns EH, Di L (2008) Drug-like properties: concepts, structure, design and methods—from ADME to toxicity optimization. Elsevier Inc, Amsterdam
16. Antoine Daina A, Olivier Michielin O, Vincent Zoete V (2017) SwissADME: a free web tool to evaluate pharmacokinetics, drug-likeness and medicinal chemistry friendliness of small molecules. Sci Rep 7:42717
17. Schuster D, Laggner C, Steindl TM, Palusczak A, Hartmann RW, Langer T (2006) Pharmacophore modeling and in silico screening for new P450 19 (aromatase) inhibitors. J Chem Inf Model 46(3):1301–1311
18. Neves MA, Dinis TC, Colombo G, Sá e Melo ML (2009) Fast three dimensional pharmacophore virtual screening of new potent non-steroid aromatase inhibitors. J Med Chem 52(1):143–150
19. Neves MA, Dinis TC, Colombo G, Sá e Melo ML (2009) An efficient steroid pharmacophore-based strategy to identify new aromatase inhibitors. Eur J Med Chem 44(10):4121–4127
20. Ghosh D, Griswold J, Erman M, Pangborn W (2010) X-ray structure of human aromatase reveals an androgen-specific active site. J Steroid Biochem Mol Biol 118(4–5):197–202
21. Roy PP, Roy K (2010) Molecular docking and QSAR studies of aromatase inhibitor androstenedione derivatives. J Pharm Pharmacol 62:1717–1728
22. Ghosh D, Lo J, Morton D, Valette D, Xi J, Griswold J, Hubbell S, Egbuta C, Jiang W, An J, Davies HM (2012) Novel aromatase inhibitors by structure-guided design. J Med Chem 55:8464–8476
23. Bonfield K, Amato E, Bankemper T, Agard H, Steller J, Keeler JM, Roy D, McCallum A, Paula S, Ma L (2012) Development of a new class of aromatase inhibitors: design, synthesis and inhibitory activity of 3-phenylchroman-4-one (isoflavanone) derivatives. Bioorg Med Chem 20:2603–2613
24. Xie H, Qiu K, Xie X (2014) 3D QSAR studies, pharmacophore modeling and virtual screening on a series of steroidal aromatase inhibitors. Int J Mol Sci 15:20927–20947
25. Lee S, Barron MG (2015) Development of 3D-QSAR model for acetylcholinesterase inhibitors using a combination of fingerprint, molecular docking, and structure-based pharmacophore approaches. Toxicol Sci 148:60–70
26. Chen S, Hsieh JH, Huang R, Sakamuru S, Hsin LY, Xia M, Shockley KR, Auerbach S, Kanaya N, Lu H, Svoboda D, Witt KL, Merrick BA, Teng CT, Tice RR (2015) Cell-based high-throughput screening for aromatase inhibitors in the Tox21 10 K library. Toxicol Sci 147:446–457
27. Ghodsi R, Hemmateenejad B (2016) QSAR study of diarylalkylimidazole and diarylalkyltriazole aromatase inhibitors. Med Chem Res 25:834–842
28. Lee S, Barron MG (2016) A mechanism-based 3D-QSAR approach for classification and prediction of acetylcholinesterase inhibitory potency of organophosphate and carbamate analogs. J Comput Aided Mol Des 30:347–363
29. Prior AM, Yu X, Park E-J, Kondratyuk TP, Lin Y, Pezzuto JM, Sun D (2017) Structure-activity relationships and docking studies of synthetic 2-arylindole derivatives determined with aromatase and quinine reductase 1. Bioorg Med Chem Lett 27:5393–5399
30. Mojaddami A, Sakhteman A, Fereidoonnezhad M, Faghih Z, Najdian A, Khabnadideh S, Sadeghpour H, Rezaei Z (2017) Binding mode of triazole derivatives as aromatase inhibitors based on docking, protein ligand interaction fingerprinting, and molecular dynamics simulation studies. Res Pharm Sci 12(1):21–30
31. Akram M, Waratchareeyakul W, Haupenthal J, Hartmann RW, Schuster D (2017) Pharmacophore modeling and in silico/in vitro screening for human cytochrome P450 11B1 and cytochrome P450 11B2 inhibitors. Front Chem 5:104
32. Lee S, Barron MG (2018) 3D-QSAR study of steroidal and azaheterocyclic human aromatase inhibitors using quantitative profile of protein–ligand interactions. J Cheminform 10:2
33. Wadood A, Ahmed N, Shah L, Ahmad A, Hassan H, Shams S (2013) In-silico drug design: an approach which revolutionarised the drug discovery process. OA Drug Des Deliv 1(1):3
34. Sliwoski G, Kothiwale S, Meiler J, Lowe EW Jr (2014) Computational methods in drug discovery. Pharmacol Rev 66(1):334–395
35. Mallipeddi PL, Kumar G, White SW, Webb TR (2014) Recent advances in computer-aided drug design as applied to anti-influenza drug discovery. Curr Top Med Chem 14(16):1875–1889
36. Leelananda SP, Lindert S (2016) Computational methods in drug discovery. Beilstein J Org Chem 12:2694–2718
37. Katsila T, Spyroulias GA, Patrinos GP, Matsoukas M-T (2016) Computational approaches in target identification and drug discovery. Comput Struct Biotechnol J 14:177–184
38. Knight-Schrijver VR, Chelliah V, Cucurull-Sanchez L, Le Novère N (2016) The promises of quantitative systems pharmacology modelling for drug development. Comput Struct Biotechnol J 14:363–370
39. Shoichet BK (2004) Virtual screening of chemical libraries. Nature 432(7019):862–865
40. Banegas-Luna A-J, Cerón-Carrasco JP, Pérez-Sánchez H (2018) A review of ligand-based virtual screening web tools and screening algorithms in large molecular databases in the age of big data. Future Med Chem 10(22):2641–2658. https://doi.org/10.4155/fmc-2018-0076
41. Huang H, Zhang G, Zhou Y, Lin C, Chen S, Lin Y, Mai S, Huang Z (2018) Reverse screening methods to search for the protein targets of chemopreventive compounds. Front Chem 6:138
42. Kolb HC, Finn MG, Sharpless KB (2001) Click chemistry: diverse chemical function from a few good reactions. Angew Chem Int Ed 40(11):2004–2021
43. Moses JE, Moorhouse AD (2007) The growing applications of click chemistry. Chem Soc Rev 36:1249–1262
44. Hein CD, Liu X-M, Wang D (2008) Click chemistry, a powerful tool for pharmaceutical sciences. Pharm Res 10:2216–2230
45. Thirumurugan P, Matosiuk D, Jozwiak K (2013) Click chemistry for drug development and diverse chemical–biology applications. Chem Rev 113(7):4905–4979
46. Durrant JD, McCammon JA (2012) AutoClickChem: click chemistry in silico. PLoS Comput Biol 8(3):e1002397
47. Meng X-Y, Zhang X-H, Mezei M, Cui M (2011) Molecular Docking: a powerful approach for structure-based drug discovery. Curr Comput Aided Drug Des 7:146–157
48. Cavasotto CN, Adler NS, Aucar MG (2018) Quantum chemical approaches in structure-based virtual screening and lead optimization. Front Chem 6:188
49. Ryde U, Söderhjelm P (2016) Ligand-binding affinity estimates supported by quantum-mechanical methods. Chem Rev 116:5520–5566
50. Yilmazer ND, Korth M (2016) Prospects of applying enhanced semi-empirical QM methods for 2101 virtual drug design. Curr Med Chem 23:2101–2111
51. Hollingsworth SA, Dror RO (2018) Molecular dynamics simulation for all. Neuron 99:1129–1143
52. Lipinski CA, Lombardo F, Dominy BW, Feeney PJ (2001) Experimental and computational approaches to estimate solubility and permeability in drug discovery and development settings. Adv Drug Deliv Rev 46(1–3):3–26
53. Stewart JJP (2013) Optimization of parameters for semiempirical methods VI: more modifications to the NDDO approximations and re-optimization of parameters. J Mol Model 19(1):1–32
54. Irwin JJ, Sterling T, Mysinger MM, Bolstad ES, Coleman RG (2012) ZINC: a free tool to discover chemistry for biology. J Chem Inf Model 52(7):1757–1768

55. Sander T, Freyss J, von Korff M, Rufener C (2015) DataWarrior: an open-source program for chemistry aware data visualization and analysis. J Chem Inf Model 55(2):460–473
56. Berman HM, Westbrook J, Feng Z, Gilliland G, Bhat TN, Weissig H, Shindyalov IN, Bourne PE (2000) The protein data bank. Nucl Acids Res 28:235–242
57. Handoko SD, Ouyang X, Su CTT, Kwoh CK, Ong YS (2012) QuickVina: accelerating AutoDock Vina using gradient-based heuristics for global optimization. IEEE/ACM Trans Comput Biol Bioinform 9(5):1266–1272
58. Wishart DS, Knox C, Guo AC, Shrivastava S, Hassanali M, Stothard P, Chang Z, Woolsey J (2006) DrugBank: a comprehensive resource for in silico drug discovery and exploration. Nucl Acids Res 34(Database issue):D668–D672
59. Wishart DS, Feunang YD, Guo AC, Lo EJ, Marcu A, Grant JR, Sajed T, Johnson D, Li C, Sayeeda Z, Assempour N, Iynkkaran I, Liu Y, Maciejewski A, Gale N, Wilson A, Chin L, Cummings R, Le D, Pon A, Knox C, Wilson M (2017) DrugBank 5.0: a major update to the DrugBank database for 2018. Nucl Acids Res 46:D1074–D1082. https://doi.org/10.1093/nar/gkx1037
60. Open Babel, the open source chemistry toolbox. http://openbabel.org/wiki/Main_Page. Accessed 7 Feb 2019
61. Rappe AK, Casewit CJ, Colwell KS, Goddard WA III, Skiff WM (1992) UFF, a full periodic table force field for molecular mechanics and molecular dynamics simulations. J Am Chem Soc 114(25):10024–10035
62. Stewart JJP (2016) MOPAC2016. Stewart Computational Chemistry, Colorado Springs, Google Scholar
63. Klamt A, Schüürmann G (1993) COSMO: a new approach to dielectric screening in solvents with explicit expressions for the screening energy and its gradient. J Chem Soc Perkin Trans 2(5):799–805
64. Klamt A (2005) From quantum chemistry to fluid phase thermodynamics and drug design. Elsevier, Boston. ISBN 9780444519948
65. Klamt A, Moya C, Palomar J (2015) A comprehensive comparison of the IEFPCM and SS(V)PE continuum solvation methods with the COSMO approach. J Chem Theory Comput 11(9):4220–4225
66. Høyvik I-M, Jansik B, Jørgensen P (2012) Trust region minimization of orbital localization functions. J Chem Theory Comput 8:3137–3146
67. Lehtola S, Jónsson H (2013) Unitary optimization of localized molecular orbitals. J Chem Theory Comput 9(12):5365–5372
68. Durrant JD, McCammon JA (2011) BINANA: a novel algorithm for ligand-binding characterization. J Mol Graph Model 29:888–893
69. McDonald IK, Thornton JM (1994) Satisfying hydrogen bonding potential in proteins. J Mol Biol 238:777–793
70. Pettersen EF, Goddard TD, Huang CC, Couch GS, Greenblatt DM, Meng EC, Ferrin TE (2004) UCSF Chimera—a visualization system for exploratory research and analysis. J Comput Chem 13:16051–16612
71. Durrant JD, McCammon JA (2011) NNScore 2.0: a neural-network receptor–ligand scoring function. J Chem Inf Model 51(11):2897–2903
72. Case DA, Darden TA, Cheatham TE III, Simmerling CL, Wang J, Duke RE et al (2010) AMBER 11. University of California, San Francisco
73. Wang J, Wolf RM, Caldwell JW, Kollman PA, Case DA (2004) Development and testing of a general amber force field. J Comput Chem 25:1157–1174
74. AMBER parameter database. http://research.bmh.manchester.ac.uk/bryce/amber/. Accessed 20 June 2019
75. Jorgensen WL, Chandrasekhar J, Madura JD, Impey RW, Klein ML (1983) Comparison of simple potential functions for simulating liquid water. J Chem Phys 79:926–935
76. Ryckaert JP, Ciccotti G, Berendsen HJC (1977) Numerical integration of the Cartesian equations of motion of a system with constraints: molecular dynamics of *n*-alkanes. J Comput Phys 23:327–341
77. Essmann U, Perera L, Berkowitz ML, Darden T, Lee H, Pedersen LG (1995) A smooth particle mesh Ewald method. J Chem Phys 103:8577–8593
78. Sun H, Li Y, Tian S, Xu L, Hou T (2014) Assessing the performance of MM/PBSA and MM/GBSA methods. 4. Accuracies of MM/PBSA and MM/GBSA methodologies evaluated by various simulation protocols using PDBbind data set. Phys Chem Chem Phys 16:16719–16729
79. Xu L, Sun H, Li Y, Wang J, Hou T (2013) Assessing the performance of MM/PBSA and MM/GBSA methods. 3. The impact of force fields and ligand charge models. J Phys Chem B 117:8408–8421
80. Sun H, Li Y, Shen M, Tian S, Xu L, Pan P, Guan Y, Hou T (2014) Assessing the performance of MM/PBSA and MM/GBSA methods. 5. Improved docking performance using high solute dielectric constant MM/GBSA and MM/PBSA rescoring. Phys Chem Chem Phys 16:22035–22045
81. Lindorff-Larsen K, Piana S, Palmo K, Maragakis P, Klepeis JL, Dror RO, Shaw DE (2010) Improved side-chain torsion potentials for the Amber ff99SB protein force field. Proteins 78:1950–1958
82. Zheng H, Langner KM, Shields GP, Hou J, Kowiel M, Allen FH, Murshudov G, Wladek Minor W (2017) Data mining of iron(II) and iron(III) bond-valence parameters, and their relevance for macromolecular crystallography. Acta Crystallogr D Struct Biol 73:316–325
83. Kao YC, Korzekwa KR, Laughton CA, Chen S (2001) Evaluation of the mechanism of aromatase cytochrome P450. A site-directed mutagenesis study. Eur J Biochem 268(2):243–251
84. Hong Y, Rashid R, Chen S (2011) Binding features of steroidal and nonsteroidal inhibitors. Steroids 76(8):802–806
85. Adamchik S, Gilep A, Ivanchik A, Kisel M, Mihalchuk A, Rohava A, Sushko T, Usanov S, Yantsevich A (2016) Synthesis and properties of new triazole aromatase inhibitors. Proc Belarusian State Univ 11(1):280–290 **(in Russian)**
86. Jones JP, Joswig-Jones CA, Hebner M, Chu Y, Koop DR (2011) The effects of nitrogen–heme–iron coordination on substrate affinities for cytochrome P450 2E1. Chem Biol Interact 193(1):50–56
87. Sharma G, First EA (2009) Thermodynamic analysis reveals a temperature-dependent change in the catalytic mechanism of *Bacillus stearothermophilus* tyrosyl-tRNA synthetase. J Biol Chem 284:4179–4190
88. Christensen AS, Kubař T, Cui Q, Elstner M (2016) Semiempirical quantum mechanical methods for noncovalent interactions for chemical and biochemical applications. Chem Rev 116:5301–5337
89. Sulimov AV, Kutov DC, Katkova EV, Sulimov VB (2017) Combined docking with classical force field and quantum chemical semiempirical method PM7. Adv Bioinform 5:1–6
90. Blakemore DC, Luis Castro L, Churcher I, Rees DC, Thomas AW, Wilson DM, Wood A (2018) Organic synthesis provides opportunities to transform drug discovery. Nat Chem 10:383–394
91. Durrant JD, Amaro RE, McCammon JA (2009) AutoGrow: a novel algorithm for protein inhibitor design. Chem Biol Drug Des 73:168–178
92. Durrant JD, Lindert S, McCammon JA (2013) AutoGrow 3.0: an improved algorithm for chemically tractable, semi-automated protein inhibitor design. J Mol Graph Model 44:104–112